Hydrol. Earth Syst. Sci. Discuss., 10, 14189–14227, 2013
www.hydrol-earth-syst-sci-discuss.net/10/14189/2013/
doi:10.5194/hessd-10-14189-2013

Hydrology and Earth System Sciences Discussions
Open Access

Climate change impacts on the hydrologic regime of a Canadian river: comparing uncertainties arising from climate natural variability and lumped hydrological model structures

G. Seiller and F. Anctil

Chaire de recherche EDS en prévisions et actions hydrologiques, Université Laval, Département de génie civil et de génie des eaux, 1065, avenue de la Médecine, Québec, Qc, G1V0A6, Canada

Received: 31 October 2013 – Accepted: 3 November 2013 – Published: 19 November 2013

Correspondence to: G. Seiller (gregory.seiller.1@ulaval.ca)

Published by Copernicus Publications on behalf of the European Geosciences Union.

Abstract

Diagnosing the impacts of climate change on water resources is a difficult task pertaining to the uncertainties arising from the different modeling steps. Lumped hydrological model structures contribute to this uncertainty as well as the natural climate variability, illustrated by several members from the same Global Circulation Model. In this paper, the hydroclimatic modeling chain consist of twenty-four potential evapotranspiration formulations, twenty lumped conceptual hydrological models, and seven snowmelt modules. These structures are applied on a natural Canadian sub-catchment to address related uncertainties and compare them to the natural variability as depicted by five climatic members. Uncertainties are commented on the observation period and on simulated and projected climates. They rely on interannual hydrographs and hydrological indicators analysis. Results show that the natural climate variability is the major source of uncertainty, followed by the potential evapotranspiration formulations and hydrological models. The selected snowmelt modules, however, do not contribute much to the uncertainty. The analysis also illustrates that the streamflow simulation over the current climate period is already conditioned by tools' selection, propagating this uncertainty on reference and future projection, while climatic members add over it. These findings demonstrate the importance of opting for several climatic members to encompass the important uncertainty related to the climate natural variability, but also of selecting multiple modeling tools to provide a trustworthy diagnosis of the impacts of climate change on water resources.

1 Introduction

The modeling of climate change impacts on water resources remains a major challenge encompassing numerous uncertainties, from the definition of a greenhouse gas scenario to the calculation of the hydrological projection. Every modeling tool involved in this process can potentially affect our ability to render a precise diagnosis of the future.

Quantifying the uncertainties associated to the modeling of climate change impacts asks for a consistent and documented approach, reflecting the state of the scientific knowledge (Kiparsky and Gleick, 2004; Dettinger, 2005; Maurer, 2007). These uncertainties may be separated into two components: "incomplete" knowledge, reflected by model conceptualization, and "unknowable" knowledge, related to human and climate system behaviors (Carter et al., 1999). Among the four levels of climate change impacts modeling uncertainties (Boé et al., 2009), three are associated to future climate calculations (gas emissions scenarios, global climate modeling, and downscaling) and one, to hydrological modeling. Several studies addressed all of them (e.g. Kay et al., 2006; Vicuna et al., 2007; Minville et al., 2008; Boyer et al., 2010; Görgen et al., 2010; Teng et al., 2012; Jung et al., 2012) while others focused on specific ones (e.g. Ludwig et al., 2009; Gardner, 2009; Poulin et al., 2011; Bae et al., 2011; Teng et al., 2012; Velázquez et al., 2013). However, all these works are based on ensemble intercomparison and advocate the necessity of assessing uncertainties before, for example, comparing river discharges over reference (REF) and future (FUT) periods.

For instance, Kay et al. (2006) compared six different sources of uncertainty: gas emissions scenarization, global climate modeling (GCM), climate downscaling, natural variability (which is disclosed calculating GCM runs from slightly modified initial conditions), and hydrological model structures and parameters. They found that all contribute to the global uncertainty and that the GCM are the most uncertain. Minville et al. (2008) arrived to similar conclusions: GCM initiate an important part of the uncertainty but so does, to a lesser extent, climate downscaling and hydrological modeling. For their part, Teng et al. (2012) exploited fifteen GCM and operated five hydrological model structures to show that the uncertainty deriving from the hydrological modeling should not be disregarded. Conclusions shared by Prudhomme et al. (2003), Vicuna et al. (2007), Boé et al. (2009), Quintana Seguí et al. (2010), and others.

HESSD
10, 14189–14227, 2013

Hydrologists continue improving their models, yet the role of the model structures in climate change impacts studies is still little known. Intercomparison studies offer a simple mean for unraveling uncertainties associated to the many hydrological structures and concepts. As an example, Ludwig et al. (2009) focused on uncertainties emanating from hydrological modeling, comparing structures of different complexity. They confirmed the importance of the climatic projection uncertainty (i.e. scenarios, GCM, downscaling) but also stressed that hydrological modeling tools must be carefully evaluated and that a coherent protocol must be developed. Poulin et al. (2011) identified equifinal parameter sets for two hydrological structures implemented on a Canadian catchment. They concluded that model structures and parameter identification are important sources of uncertainty under a changing climate. Velázquez et al. (2013) confirmed that the selection of a hydrological model affects climate change impacts conclusions, especially for low flows on two dissimilar catchments, in Germany and Canada.

Many hydrological models resort to a simplistic approach to simulate the actual evapotranspiration, namely to an agronomic concept called potential evapotranspiration (PET), representative of constant crop and soil conditions. PET formulations are largely influenced by a changing climate (changes in the evaporative demand) and are thus a supplemental source of uncertainty. However, scant researches address this question even if the diversity of PET formulations and concepts is compatible for intercomparison. As an example, Kay and Davies (2008) found that Penman equation compared to a simple temperature-based formulation (Oudin et al., 2005) in a climate change context with A2 scenario, both offer very different results for climate change impacts modeling on water resources for the 2071–2100 period. They advised that the choice of a PET formulation affects hydrological projections. Bae et al. (2011) evaluated uncertainties from hydrological models and PET formulations on a Korean catchment. They confronted three hydrological models, three PET formulations, and thirty-nine climate scenarios for the 2020 and 2080 horizons. Their results showed that hydrological modeling affects global uncertainty, revealing the importance of the PET formulation and demonstrating the need to account for them in climate change impacts assessment

HESSD
10, 14189–14227, 2013

projects. More, Bormann (2011) compared eighteen PET computations over six German meteorological stations and found a large sensitivity to climate.

The authors are aware of no work addressing the hydrological projections uncertainty emanating from lumped snow modules, but the literature targeting snow melt (e.g. WMO, 1986; Valéry, 2010; Franz et al., 2010) reported large uncertainties on the simulated discharge. It is thus expected that this variability remains at least as important under changing climate.

In this work, PET formulations, snow modules, and lumped hydrological structures are compared under climate change, along with the natural variability of the climate system. Climate simulation ensembles allow the analysis of their natural variability and can be seen as the irreducible fraction of climate simulations uncertainty (Velázquez et al., 2013), a part of the "unknowable" knowledge stated above. Climatic reference simulations (REF) and future projections (FUT) may then vary substantially from one member of the ensemble to the other. Indeed, the chaotic nature of the climate produces dissimilar time series when a GCM is initiated with slightly modified initial conditions, here in 1850. The natural climate uncertainty, described by climatic members (C1 to C5), will thus serve as benchmark for the other explored sources of uncertainty.

More specifically, this project confronts uncertainties related to the natural climate variability and to lumped hydrological model structures, in the context of climate change impact on the hydrologic regime of a Canadian river. It will confer on our ability to render a diagnosis of climate change impacts on the water resources of the *au Saumon* catchment.

Section 2 outlines the methodology, the *au Saumon* catchment, the data, as well as the modeling tools. Section 3 presents and details the results, followed by conclusions and discussion in the Sect. 4.

HESSD
10, 14189–14227, 2013

2 Material and methods

2.1 The *au Saumon* catchment

The *Haut-Saint-François* catchment drains a 2940 km^2 territory located 120 km south of Quebec City and 200 km east of Montreal. It fosters three dams for flood control, environmental needs, recreational activities, and water consumption – the lower one is mostly dedicated to hydroelectric production. The natural *au Saumon* (SAU) subcatchment, upstream the *Haut-Saint-François* River, receives waters from a 738 km^2 area along a south/south-east to north/north-west path. Figure 1 details this location and its geographic characteristics. The hydrographic network is dense and uniformly distributed, altitudes range from 277 and 1092 m, land use is dominated by mixed coniferous/deciduous forests and agricultural lands, while the geology is dominated by limestone, sandstone, and shale. The hydrologic regime is characterized by an important spring freshet (from March to May) and high autumnal flows.

2.2 Hydrological, meteorological and climatic data

Hydrological and meteorological data are provided by the *Centre d'expertise hydrique du Québec*. Hydrometrical data correspond to daily discharges from the *au Saumon* gauging station (1975 to 2003). The annual mean discharge reaches 771 mm (approximately 18 m^3 s^{-1} on an average day).

Meteorological observations consist in daily mean, minimum and maximum air temperatures (°C), daily total precipitation (mm), incoming solar radiation (W m^{-2}), relative humidity (%), and wind speed at 2 m (m s^{-1}). Radiation, humidity and wind speed measurements originate from the nearby Sherbrooke station, outside of the watershed. All data are spatially lumped over the catchment and extend from 1975 to 2003. Mean temperature attains 4.5 °C but only −11 °C in January. Precipitation is quite uniform over the year and averages 1284 mm, with 355 mm as solid precipitation. Maximal incoming solar radiation occurs in June (246 W m^{-2}) while the relative daily humidity

HESSD
10, 14189–14227, 2013

fluctuates between 73 % (April) and 85 % (September). Average wind oscillates from $2\,m\,s^{-1}$ (August) to $3.5\,m\,s^{-1}$ (March).

Climatic data originated from the Canadian Global Climate Model (CGCM version 3 with a 3.75° resolution, Scinocca et al., 2008), fed with SRES A2 scenario (Nakicenovic et al., 2000). Data were dynamically downscaled by the Canadian Regional Climate Model (CRCM version 4.2.3, de Elía and Côté, 2010). The CRCM domain consisted of 111 × 87 grid points with a 45 km resolution (true at 60° N) centered on the Province of Quebec.

Downscaled climatic data were provided by Consortium Ouranos: reference simulations (REF) cover 1971 to 2000 while future projections (FUT), 2041 to 2070 (2050s horizon). The climate natural variability is depicted by five climatic members (C1 to C5) that were bias-corrected to reduce deviation between REF and observations on precipitation and temperature. Monthly correction factors were computed for each climatic member on the 30 yr monthly average minimum and maximum temperatures and were applied on each member to preserve their respective variance. Precipitation was corrected using the LOCal Intensity (LOCI) scaling method (Schmidli et al., 2006), adjusting mean monthly precipitation in terms of frequencies and intensity over 30 yr. This procedure hypothesizes that these corrections are maintained in future climate. Monthly average FUT temperature time series increase between 2 and 3 °C, without much variability between climatic members. Precipitation highlights a larger variability than temperature, from one climatic member to the other. Projected precipitation changes are substantial, increasing mostly from October to May and decreasing in summer. Incoming solar radiation slightly increases on FUT from June to August and relative humidity is mostly unchanged, with a small increase in March. Wind speed slightly increases in FUT (maximum $+0.8\,m\,s^{-1}$).

2.3 Hydroclimatic modeling chain

The main objective of this intercomparison consists in evaluating multiple representations of hydrological modeling behaviors, beyond the pre-supposed most appropriate model, because models are conceptualisations of real systems. It would then be possible to evaluate and quantify structural uncertainties in a climate change context. The issue is to select relevant hydrological modeling tools in terms of number, diversity and pertinence, since they must be hypothetically appropriate for simulating catchment flows and must be known for their performance.

2.3.1 Twenty lumped conceptual hydrological models

Researches led by Perrin et al. (2001, 2003) and by Mathevet (2005) provide a hefty source of information on lumped conceptual hydrological models. It concerns a large number of rainfall–runoff structures, tested on numerous watersheds, exploiting diverse rainfall–runoff transformation concepts and soil moisture accounting processes (e.g. linear, non-linear, multilayer, etc.). They are also designed to take into account many contributions to the total flow, based on storages (also called buckets) and interconnections, as well as flow routing delay (e.g. unit hydrogram, time laps, etc.). In some cases, when the sensitivity was considered small, their designers have fixed some of their parameters in order to favour the parsimony of the models, reducing computation time and equifinality issues. These models, or part of, were exploited by Velázquez et al. (2010) for exploring multimodel ensemble forecasting and by Seiller et al. (2012) for assessing the robustness of the ensemble under contrasted climate.

Twenty conceptual lumped hydrological models (M01 to M20) are tested (see Table 1). They rely on four to ten free parameters and on two to seven storages – the number of storages correspond to the ones structuring the model and consequently they do not all participate directly to the routing. In the same way, it was recognised that interception function can be assimilated as a "surface storage". Figure 2 illustrates the structural diversity of the selected models. It informs on their inputs and output, as well as on the different types of storages: surface, soil, root zone, groundwater, main routing, delayed routing, etc. All models were applied in exactly the same conditions and run at a daily time step.

HESSD
10, 14189–14227, 2013

2.3.2 Twenty-four potential evapotranspiration formulations

Oudin et al. (2005) and Xu and Singh (1997, 1998, 2000, 2001, 2002) provided a great source of inspiration for PET formulation selection. For instance, Oudin et al. (2005) implemented 27 PET formulations and four hydrological models on 308 catchments of diverse hydroclimatic conditions.

Twenty-four PET formulations (E01 to E24), adapted to our hydroclimatic context, were selected for this study. They are of three types: combinational (six), temperature-based (eight), and radiation-based (ten). Figure 3 lists the formulas and related input data. Classification into families depends on the development philosophy more than their input data. For example, Priestley–Taylor formula (E04) is combinational even if wind speed is not explicitly used as an input, because it is a simplification of Penman formula (E01). On the opposite, Doorenbos–Pruitt formula (E20) is an adaptation of radiation-based formula E22 (Makkink), even if wind speed is used as an input data. All of them originate from various regional contexts and development objectives, but our selection aims to cover a large spectrum of concepts in order to favour diversity.

Empirical coefficients have been set for the *au Saumon* catchment, based on recent developments and applications. Shared parameters or variables have been computed based on EWRI-ASCE report recommendations (Allen et al., 2005).

2.3.3 Seven snow modules

Valéry (2010) studied existing snow modules from a hydrological (streamflow) point of view, before proposing a novel one: CemaNeige. The latter originates from a comprehensive database composed of 380 watersheds exposed to diverse Nordic meteorological and geographical conditions in Sweden, France, Canada, and Switzerland. Parsimony, performance and robustness were the main objectives of the CemaNeige development.

The degree-day based CemaNeige (Valéry, 2010; Nicolle et al., 2011) relies on two free-parameters: K_f, the melting rate (mm °C^{-1}) and C_{Tg}, the snowpack thermal state coefficient (no unit), and on two state variables: G, the snowpack in mm and eTg, the snowpack thermal state in °C. CemaNeige exploits five altitudinal layers of equal area. Its precipitation partition, between solid and liquid, alternates between two formulations depending on the layer altitude. Liquid precipitation is directly by-passed to the hydrological model, whereas solid precipitation is cumulated in the snowpack G. The thermal state of the snowpack is calculated with air temperature and C_{Tg} coefficient. Melt depends on degree-day and is only activated when temperature is above the melt temperature (fixed at 0 °C) and depending on the K_{f} parameter. Effective melt (mm day^{-1}) is inputted to the hydrological model.

Valéry's thesis details the many concepts and structures considered during the development process of CemaNeige (N1). Inspired by a parsimonious bottom-up point of view, a concept or structure was only retained in CemaNeige if it substantially improved the hydrological performance over most of the 380 tested watersheds. It is thus opted in the present study to explore some of these rejected concepts, functions, and parameters in order to develop six alternative snow modules (N2 to N7) of various structural levels of complexity. Individual concepts (i.e. air temperature, melt temperature, precipitation separation, melting rate, melt weighting, altitudinal layering, thermal state, melt routing, precipitation correction, liquid water retention, and heat due to rain) were confronted in order to compile the six new versions (see Fig. 4 and Table 2). Selection is a compromise between performance (close or above CemaNeige' ones for the *au Saumon* catchment) and internal diversity (snowpack, solid precipitations, thermal state, and effective melt).

2.4 Model calibration

Hydrological models calibration is achieved over the entire observed dataset (i.e. from 1975 to 2003) – differential split sample tests were performed in Seiller et al. (2012). It relies on the Shuffled Complex Evolution (SCE) algorithm (Duan and Gupta, 1992; Duan et al., 1994), a robust heuristic automatic optimisation tool (error minimisation) that is common in hydrological sciences and is known for its performance (e.g. Wang

Discussion Paper | Discussion Paper | Discussion Paper | Discussion Paper |

HESSD

10, 14189–14227, 2013

Climate change impacts on the hydrologic regime of a Canadian river

G. Seiller and F. Anctil

et al., 2009). The SCE proceeds in five steps over the entire parametric space by generating an initial parameter population, ranking results, partitioning into complexes, evolving complexes, and recombining them until the convergence criteria is reached. Here, the objective function is the Nash–Sutcliffe efficiency (Nash and Sutcliffe, 1970) computed on root-squared discharges (NSE_{sqrt}):

$$NSE_{sqrt} = 1 - \frac{\sum_{i=1}^{N}\left(\sqrt{Q_{sim,i}} - \sqrt{Q_{obs,i}}\right)^2}{\sum_{i=1}^{N}\left(\sqrt{Q_{obs,i}} - \overline{\sqrt{Q_{obs}}}\right)^2} \quad (1)$$

with $Q_{obs,i}$ and $Q_{sim,i}$ respectively the observed and simulated discharges at time step i and N the total number of observations. Criteria on root-squared discharges are considered as multi-purpose, evaluating global deviation between observed and simulated discharges with a lesser emphasis on high flow discharges than the standard NSE on non-transformed discharges (Chiew and McMahon, 1994; Oudin et al., 2006).

3360 calibrated parameter sets (i.e. one for each hydrological model/PET/snow module combination) are then available for reference simulations (REF, 1970–2000) and future projections (FUT, 2041–2070). Such methodology assumes that the parameter sets are compatible for current and future climatic conditions, addressing the issue of transposability. Transposability in time, on contrasted climatic conditions, is discussed for the same catchment and models in Seiller et al. (2012).

2.5 Hydroclimatic simulations and projections

Current simulations (or calibration, CAL), reference simulations (REF) and future projections (FUT) consist in a large number of time series. They exploit the 3360 parameter sets, which lead to:

- 3360 simulations (20M × 24E × 7N) for the observed period;

HESSD
10, 14189–14227, 2013

– 16 800 simulations (20M × 24E × 7N × 5C) for the reference period;

– 16 800 projections (20M × 24E × 7Nx 5C) for the future period.

Together, they form the basis of the present uncertainty assessment. Hydrographs and indicators (overall mean flow) on current period simulations (CAL) illustrate the uncertainty of the modeling process, whereas comparison between reference (REF) and future (FUT) time series highlights the influences of climate change on water resources, but mostly evaluates the uncertainty in our diagnosis, related to hydrological modeling and natural variability.

3 Results

3.1 Calibration performance

Table 3 synthetizes the outcome of the calibration in terms of NSE_{sqrt} for each hydrological tool, providing median values and 5th and 95th percentiles (in brackets). The hydrological model section (M01 to M20) pools 168 values per model, the PET formulation section (E01 to E24) embeds 140 values per formulation, while the snow module section (N1 to N7) groups 480 values per module. The best performance is achieved by M05, with a median NSE_{sqrt} of 0.81, while M02 (0.56) and M13 (0.57) rank last. E12 (0.66) is the less efficient PET formulation while E23 (0.78) is prevalent. It should be highlighted that PET performance is less contrasted than for the hydrological models. Snow modules are quite uniform in terms of performance (0.75), except N7 that is lesser (0.71). The overall performance is quite satisfying and shows a great adequacy between the observed and simulated discharge on the *au Saumon* catchment.

HESSD

10, 14189–14227, 2013

Climate change impacts on the hydrologic regime of a Canadian river

G. Seiller and F. Anctil

3.2 Cumulative streamflow uncertainty

3.2.1 Observation simulation

Assessment of the observation total cumulative uncertainty illustrates the diversified response of our individual modeling tools on a period for which discharges are available. Initial modeling miscues may thus be identified and characterised, on an interannual average daily basis.

The cumulative uncertainty on the *au Saumon* catchment is illustrated in Fig. 5: the dark and pale blue envelopes illustrate the distribution of the streamflow ensemble (5 to 95 % and 25 to 75 %, respectively), the blue line, the median flow, and the black line, the observed flow. Envelopes are drawn connecting daily discharges, using a moving average to smoother the lines. Observations fall within the 5 to 95 % envelope except for a part of January (underestimation), a few days in September (overestimation) and from mid-November to the third week of December (underestimation). The highest uncertainty occurs during the most active hydrological period, namely the spring flood, with a maximum spread of 2.74 mm on 22 April (between 7.15 and 4.41 mm). The smallest uncertainty ensues during the winter low flows, with a minimum spread of 0.37 mm on 10 February (between 0.96 and 0.59 mm). These findings confirm that high flows are more complex to encompass than low flows, probably because of their irregular behavior. However, the choice of an objective function based on root-squared transformed discharges may also provide an explanation for this specific behavior. Still, it remains a relevant criterion for climate change impacts.

In addition, it may be helpful to explore the reliability of the quantiles' envelopes, empirically drawn from the 3360 simulations, to comment if the latter can be directly interpreted as confidence intervals. For this purpose, a confidence interval reliability diagram is computed for the *au Saumon* catchment (Fig. 6). The concept of a confidence interval reliability diagram consists in verifying if the observed relative frequency correspond to the simulated one – perfect reliability would result in a 1 : 1 slope on the diagram (Wilks, 1995). Several confidence intervals are thus plotted (from 0.1 to

0.9) with, for example, 0.5 corresponding to the quartiles spread (25 to 75 %) and 0.9 corresponding to the spread of the 5 to 95 % quantiles. Thus, for each of the 3360 simulations and each confidence interval, statement if observed discharge is included or not is verified, resulting in the reliability graph (Boucher et al., 2009; Velázquez et al., 2010). Results in Fig. 6 reveal a slight under-dispersion, confirming a possible link between the envelopes drawn in Fig. 5 and confidence intervals.

These results confirm that the ability to simulate the precipitation-runoff transformation is hampered by the choice of lumped conceptual modeling tools. However, it can be questioned if this uncertainty is maintained, reduced or increased with climatic data as inputs and if it persists in future projections, affecting de facto our ability to report a diagnosis of the impacts of climate change on water resources.

3.2.2 Climate simulation and projection

Figures 7 and 8 propose a similar hydrograph analysis for reference simulations (REF, green) and future projections (FUT, red), respectively, based on climate data. Streamflow uncertainty originates either from the hydrological modeling process or from the climate natural variability (members), as disclosed by 16 800 simulations and projections. For REF (Fig. 7), as for the observations, the largest uncertainty occurs during spring flood with a maximum spread of 3.19 mm (between 7.53 and 4.34 mm) on 26 April, while the smallest uncertainty takes place in winter, 27 December, when the spread falls to 0.56 mm (between 1.29 and 0.73 mm). For FUT (Fig. 8), the largest uncertainty (2.86 mm) is reached on 19 April, with discharge oscillating between 6.84 and 3.98 mm, and smallest uncertainty occurs 1 February, with a 0.81 mm spread (between 2.42 and 1.61 mm). REF and FUT uncertainties are more important than simulation on the observed period, but the latter do not account for the climate natural variability (members). Envelops are more uniform over the year, when including the climate natural variability.

Evolution from REF to FUT reveals a spring flood anticipated by about 15 days, with a slight decrease in the spring high flows. More, changes favour an increase of winter low flows and a decrease of summer low flows, demonstrating a substitution in time of the lowest flows.

This streamflow uncertainty analysis, based on interannual hydrographs combining the influence of the hydrological process and of the climate natural variability, reveals some adversity in our ability to produce a clear diagnosis of climate change impacts on water resources for the *au Saumon* catchment. Indeed, cumulative uncertainties envelopes are large, especially on hydrologically sensitive periods such as spring high flows and summer low flows.

3.3 Process-based streamflow uncertainty

Analysis of the cumulative uncertainty from yearly averaged hydrographs highlights the extent of the uncertainty in simulation and projection, but without providing much information about its origin. To assess this question in more details and to identify which modeling step contributed the most to the reported cumulative uncertainty, a water resources manager point of view is taken next, using a simple hydrological indicator: the overall mean flow (OMF), corresponding to averaged daily flow. A process-based streamflow uncertainty is then available, allowing comments about its extent on the observation period and about its change from REF to FUT periods.

3.3.1 Observation OMF

Figure 9 illustrates, by type of tools, the OMF uncertainty for simulations on the observation (calibration) period – blue boxplots for the lumped conceptual hydrological models (168 values per boxplot), green boxplots for the PET formulations (140 values per boxplot), and grey boxplots for the snow modules (480 values per boxplot) – while the black boxplot (3360 values) illustrates the OMF total uncertainty. In Fig. 9, colored bars indicate the 2 and 75 % quartiles of each distribution, while the horizontal white line identifies the median value. The latter can be associated to the uncertainty for each tool, while the interquartile range (e.g. blue bars for the models) can be perceived as

HESSD
10, 14189–14227, 2013

depicting sensitivity and robustness. Finally, the observed OMF (2.12 mm) is illustrated by a red cross in the total uncertainty box. The latter is higher than most of the 3360 runs because, as already mentioned in the hydrographs analysis, the observed spring high flow is in general underestimated.

M04 median OMF (2.13 mm) is quite close to the observed one. It is however the highest median OMF out of 20. The lowest one is the M12 median OMF (1.83 mm), disclosing the range of the uncertainty emanating from the lumped conceptual models and the importance of selecting the right model if exploiting only one structure. It can also be pointed out that M05 and M08 generate reduced inner sensitivity (i.e. smaller interquartile ranges), while the opposite is true for M12 and M07.

PET OMFs divulge an even higher uncertainty than for the lumped conceptual models. Indeed, their median OMF range from 2.48 mm (E02) to 1.79 mm (E20), largely encompassing the observed OMF (red cross), but also stressing the necessity of selecting an appropriate PET formulation. The PET inner sensitivity (extent of the green bar) varies also considerably from one another, the largest and smallest ranges originating from E02 and E23, respectively. Note finally that some PET OMF distributions are quite asymmetrical, namely for E01, E02, E03, E04, E06, and E10, combination formulations for most of them.

If the selection of a particular lumped conceptual model and of a particular PET formulation have a huge impact on the OMF uncertainty, it is clearly not the case for the seven selected snow modules, which interquartile ranges and median OMFs, extending from 1.96 mm (N1) to 1.95 mm (N7), are all quite similar.

3.3.2 OMF relative change

A similar analysis is performed on the OMF relative change from REF to FUT [$100 \times (\text{OMF}_{\text{FUT}} - \text{OMF}_{\text{REF}})/\text{OMF}_{\text{REF}}$, in %], drawing boxplots (Fig. 10) for each modeling process and for each climatic member (red), the latter in order to depict the climate natural variability – each member originated from the same GCM initiated with slightly modified initial conditions in 1850, expressing the chaotic nature of the climate. Total

HESSD
10, 14189–14227, 2013

OMF uncertainty then combines 16 800 relative changes, 840 ones per lumped conceptual model, 700 per PET formulation, 2400 per snow module, and finally 3360 per climatic member. Focus is again mainly given to median values (uncertainty) and interquartile ranges (inner sensitivity).

The total OMF relative change fluctuates from −11 to +129 %, but its interquartile range is restrained from +4.2 mm to +16.2 %, with a median value of +9.3 %.

The median OMF relative change per lumped conceptual model fluctuates from +16.8 (M08) to +6.3 % (M02), confirming the sensitivity to the lumped conceptual model selection. The interquartile range is more uniform from one model to the other than in Fig. 9, but M08 differs (18.1 %) in that regard – M08 was already identified with poor transposability on the same catchment by Seiller et al. (2012). The lowest inner sensitivity is achieved by M11 (10.9 %).

PET OMF relative change is in general slightly higher than for the lumped conceptual models, from +17.1 (E21) to +4.1 % (E13), stressing also the sensitivity to the selection of a PET formulation. The highest interquartile range is produced by E21 (14.5 %) and the lowest, by E02 (10.6 %).

Again, the behaviour of the snow modules is more uniform than for the lumped conceptual models and for the PET formulations. The median OMF relative change of the snow modules are restrained from +9.9 (N3) to +9.1 % (N2), while their interquartile ranges vary from 12.5 (N3) to 11.9 % (N2).

On the other hand, the behaviour of the climatic members is quite distinct. First, the interquartile ranges of their OMF relative change are much reduced when compared to the others: from 4.8 (C1) to 3.6 % (C4), expressing lower inner sensitivity. Second, their median OMF relative changes vary considerably: between +19.1 (C3) and +2.7 % (C4). This latter characteristic exemplifies the importance of the climatic natural variability. Changes differ greatly from one climatic member to the other. It is thus evident that a single 30 yr realisation of the climate is insufficient to depict all the possible variability. Furthermore, it is also striking that an important part of the uncertainty spread

HESSD
10, 14189–14227, 2013

revealed by the various hydrological processes actually originates from the climatic natural variability.

The importance of the total OMF relative change, combining 16 800 simulations and projections, stresses the limit of our ability to provide a clear diagnosis of climate change impacts on water resources, namely for the *au Saumon* catchment. From these results, climatic natural variability is the first uncertainty driver, followed by PET formulations, lumped conceptual models, and snow modules, as depicted by the standard deviations of the median OMF relative change (Table 4), with respective values of 6.9, 3.3, 2.4, and 0.3 %.

Since snow accumulation and melt are important hydrological processes on the *au Saumon* catchment, standard deviations of the median OMF relative change are also provided in Table 4 distinguishing months with mean interannual air temperature above 0 °C (April to October) from months with mean interannual air temperature below 0 °C (November to May). This distinction has only a small influence on the respective standard deviation values and none on the ranking of the uncertainty sources.

4 Discussion and conclusion

This paper explored uncertainties related to the hydrological modeling of climate change impacts on water resources. In particular, twenty lumped conceptual hydrological models, twenty-four PET formulations, and seven snow modules were assessed in order to evaluate our skill diagnosing the impacts of climate change on the hydrologic regime of a river. Natural climate variability, by the mean of climatic members, was also studied for comparison with the diverse hydrological structures.

Analysis on uncertainties illustrates that streamflow simulation over the current climate period (calibration) is already largely conditioned by hydrological tools' selection, propagating this uncertainty on reference simulation and future projection. Results indicate that the largest source of uncertainty is associated to the natural climate variability, followed by PET formulations, lumped conceptual models, and snow modules.

Calibration process and transposability questions thus appear as major issues for the calculation of future hydrological projections, but natural variability plays an even more substantial role in our ability to provide a diagnosis on the impacts of climate change on the hydrologic regime of a river, especially when exploiting hydrological indicators such as the OMF. Nonetheless, the fact that changes in the hydrologic regime of the *au Saumon* catchment differed greatly from one climatic member to the other; one has to question if a single 30 yr realisation of the climate is sufficient to encompass all the possible variability.

This work focussed on only one Canadian catchment and must be confirmed with other watersheds and climate contexts, but the proposed methodology is easily transferable. Following climate natural variability, PET formulations add to the total uncertainty in a substantial way, but without much distinction between combinational, radiation-based, and temperature-based formulations. Only lumped conceptual hydrological models were explored, mainly to limit implementation and computation time as well as parameter identification issues, but inclusion of several other model classes would be an important complementary contribution. Finally, uncertainties associated to snow modules turned out small for the current climate period as well as for the projections. It should be mentioned that the selected tools originated from the sane snow module (CemaNeige) re-designed in six other versions and that this approach may have affected the results. Here also, more diverse modules may be considered in further exploration of this issue.

Acknowledgements. The authors acknowledge NSERC, Ouranos, and Hydro-Québec for support, as well as partners in the $QBIC^3$ project.

References

Allen, R. G., Walter, I. A., Elliott, R., Howell, T., Itenfisu, D., and Jensen, M.: The ASCE standardized reference Evapotranspiration equation – Final Task Commitee Report, 70 pp., 2005.

Bae, D. H., Jung, I. W., and Lettenmaier, D. P.: Hydrologic uncertainties in climate change from IPCC AR4 GCM simulations of the Chungju Basin, Korea, J. Hydrol., 401, 90–105, 2011.

Bergström, S. and Forsman, A.: Development of a conceptual deterministic rainfall–runoff model, Nord. Hydrol., 4, 147–170, 1973.

Beven, K. J. and Kirkby, M. J.: A physically based, variable contributing area model of basin hydrology, Hydrol. Sci. Bull., 24, 43–69, 1979.

Boé, J., Terray, L., Martin, E., and Habets, F.: Projected changes in components of the hydrological cycle in French river basins during the 21st century, Water Resour. Res., 45, 1–15, 2009.

Bormann, H.: Sensitivity analysis of 18 different potential evapotranspiration models to observed climatic change at German climate stations, Clim. Change, 104, 729–753, doi:10.1007/s10584-010-9869-7, 2011.

Boucher, M.-A., Perreault, L., and Anctil, F.: Tools for the assessment of hydrological ensemble forecasts obtained by neural networks, J. Hydroinform., 11, 297–307, doi:10.2166/hydro.2009.037, 2009.

Boyer, C., Chaumont, D., Chartier, I., and Roy, A. G.: Impact of climate change on the hydrology of St. Lawrence tributaries, J. Hydrol., 384, 65–83, doi:10.1016/j.jhydrol.2010.01.011, 2010.

Burnash, R. J. C., Ferral, R. L., and McGuire, R. A.: A general streamflow simulation system: Conceptual models for digital computers, Joint-Federal State River Forecast Center, Sacramento, CA, 68 pp., 1973.

Carter, T., Hulme, M., and Viner, D.: Representing uncertainty in climate change scenarios and impact studies, in: Proceedings of the ECLAT-2 Helsinki Workshop 14–16 April 1999, Report No. 1, 128 pp., 1999.

Chiew, F. H. S. and McMahon, T. A.: Application of the daily rainfall–runoff model MODHYDROLOG to 28 Australian catchments, J. Hydrol., 153, 383–416, 1994.

Chiew, F. H. S. and Siriwardena, L.: Estimation of SIMHYD parameter values for application in ungauged catchments, in MODSIM 2005 International Congress on Modelling and Simulation, Modelling and Simulation Society of Australia and New Zealand, Melbourne, Australia, 2883–2889, 2005.

Cormary, Y. and Guilbot, A.: Étude des relations pluie-débit sur trois bassins versants d'investigation, in: IAHS Publication No. 108 – Madrid Symposium, June 1973, 265–279, Madrid, 1973.

De Elía, R. and Côté, H.: Climate and climate change sensitivity to model configuration in the Canadian RCM over North America, Meteorol. Z., 19, 325–339, doi:10.1127/0941-2948/2010/0469, 2010.

Dettinger, M. D.: From climate-change spaghetti to climate-change distributions for 21st Century California, San Fr. Estuary Watershed Sci., 3, 1–14, 2005.

Duan, Q. and Gupta, V.: Effective and efficient global optimization for conceptual rainfall–runoff models, Water Resour., 28, 1015–1031, 1992.

Duan, Q., Sorooshian, S., and Gupta, V.: Optimal use of the SCE-UA global optimization method for calibrating watershed models, J. Hydrol., 158, 265–284, 1994.

Fortin, V. and Turcotte, R.: Le modèle hydrologique MOHYSE, Environnement Canada et Centre d'expertise hydrique du Québec, Quebec city, 17 pp., 2007.

Franz, K. J., Butcher, P., and Ajami, N. K.: Addressing snow model uncertainty for hydrologic prediction, Adv. Water Resour., 33, 820–832, 2010.

Garçon, R.: Modèle global pluie-débit pour la prévision et la prédétermination des crues, Houille Blanche, 7, 88–95, 1999.

Gardner, L. R.: Assessing the effect of climate change on mean annual runoff, J. Hydrol., 379, 351–359, doi:10.1016/j.jhydrol.2009.10.021, 2009.

Girard, G., Morin, G., and Charbonneau, R.: Modèle précipitations-débits à discrétisation spatiale, Cah. ORSTOM, Série Hydrol., IX, 35–52, 1972.

Görgen, K., Beersma, J., Brahmer, G., Buiteveld, H., Carambia, M., de Keizer, O., Krahe, P., Nilson, E., Lammersen, R., Perrin, C., and Volken, D.: Assessment of climate change impacts on discharge in the Rhine river basin: Results of the RheinBlick2050 project, International Commission for the Hydrology of the Rhine Basin, 211 pp., 2010.

Jakeman, A. J., Littlewood, I. G., and Whitehead, P. G.: Computation of the instantaneous unit hydrograph and identifiable component flows with application to two small upland catchments, J. Hydrol., 117, 275–300, 1990.

Jung, I. W., Bae, D. H., and Lee, B. J.: Possible change in Korean streamflow seasonality based on multi-model climate projections, Hydrol. Process., 27, 1033–1045, doi:10.1002/hyp.9215, 2012.

Kay, A. L. and Davies, H. N.: Calculating potential evaporation from climate model data: a source of uncertainty for hydrological climate change impacts, J. Hydrol., 358, 221–239, doi:10.1016/j.jhydrol.2008.06.005, 2008.
Kay, A. L., Reynard, N. S., and Jones, R. G.: RCM rainfall for UK flood frequency estimation. I. Method and validation, J. Hydrol., 318, 151–162, doi:10.1016/j.jhydrol.2005.06.012, 2006.
Kiparsky, M. and Gleick, P. H.: Climate change and California water resources, in: The World's Water 2004–2005, edited by: Gleick, P. H., Island Press, Washington DC, 157–188, 2004.
Ludwig, R., May, I., Turcotte, R., Vescovi, L., Braun, M., Cyr, J.-F., Fortin, L.-G., Chaumont, D., and Biner, S.: The role of hydrological model complexity and uncertainty in climate change impact assessment, Adv. Geosci., 21, 63–71, 2009, http://www.adv-geosci.net/21/63/2009/.
Mathevet, T.: Quels modèles pluie-débit globaux au pas de temps horaire?, École Nationale du Génie Rural, des Eaux et des Forêts, Paris, 463 pp., 2005.
Maurer, E. P.: Uncertainty in hydrologic impacts of climate change in the Sierra Nevada, California, under two emissions scenarios, Clim. Change, 82, 309–325, 2007.
Mazenc, B., Sanchez, M., and Thiery, D.: Analyse de l'influence de la physiographie d'un bassin versant sur les paramètres d'un modèle hydrologique global et sur les débits caractéristiques à l'exutoire, J. Hydrol., 69, 97–118, 1984.
Minville, M., Brissette, F., and Leconte, R.: Uncertainty of the impact of climate change on the hydrology of a nordic watershed, J. Hydrol., 358, 70–83, 2008.
Moore, R. J. and Clarke, R. T.: A distribution function approach to rainfall runoff modeling, Water Resour. Res., 17, 1367–1382, 1981.
Nakicenovic, N., Alcamo, J., Davis, G., de Vries, B., Fenhann, J., Gaffin, S., Gregory, K., Grübler, A., Jung, T. Y., Kram, T., Lebre La Rovere, E., Michaelis, L., Mor, S., Morita, T., Pepper, W., Pitcher, H., Price, L., Riahi, K., Roehrl, A., Rogner, H.-H., Sankovski, A., Schlesinger, M., Shukla, P., Smith, S., Swart, R., van Rooijen, S., Victor, N., and Dadi, Z.: Emissions Scenarios. A Special Report of Working Group III of the Intergovernmental Panel on Climate Change, Cambridge University Press, Cambridge, UK, 2000.
Nash, J. E. and Sutcliffe, J. V.: River flow forecasting through conceptual models. Part I – a discussion of principles, J. Hydrol., 10, 282–290, 1970.
Nicolle, P., Ramos, M.-H., Andréassian, V., and Valéry, A.: Mieux prévoir les crues nivales: Évaluation de prévisions probabilistes de débit sur des bassins versants de montagne français, in

HESSD
10, 14189–14227, 2013
Climate change impacts on the hydrologic regime of a Canadian river
G. Seiller and F. Anctil

Colloque SHF: “L’eau en montagne, mieux observer pour mieux prévoir”, 163–170, Société Hydrotechnique de France, Lyon, France, 2011.
Nielsen, S. A. and Hansen, E.: Numerical simulation of the rainfall–runoff process on a daily basis, Nord. Hydrol., 4, 171–190, 1973.
O’Connell, P. E., Nash, J. E., and Farrell, J. P.: River flow forecasting through conceptual models. Part II – the Brosna catchment at Ferbane, J. Hydrol., 10, 317–329, 1970.
Oudin, L., Hervieu, F., Michel, C., Perrin, C., Andréassian, V., Anctil, F., and Loumagne, C.: Which potential evapotranspiration input for a lumped rainfall–runoff model? Part 2 – towards a simple and efficient potential evapotranspiration model for rainfall–runoff modelling, J. Hydrol., 303, 290–306, 2005.
Oudin, L., Andréassian, V., Mathevet, T., Perrin, C., and Michel, C.: Dynamic averaging of rainfall-runoff model simulations from complementary model parameterizations, Water Resour. Res., 42, W07410, doi:10.1029/2005WR004636, 2006.
Perrin, C., Michel, C., and Andréassian, V.: Does a large number of parameters enhance model performance? Comparative assessment of common catchment model structures on 429 catchments, J. Hydrol., 242, 275–301, 2001.
Perrin, C., Michel, C., and Andréassian, V.: Improvement of a parsimonious model for streamflow simulation, J. Hydrol., 279, 275–289, doi:10.1016/S0022-1694(03)00225-7, 2003.
Poulin, A., Brissette, F., Leconte, R., Arsenault, R., and Malo, J.-S.: Uncertainty of hydrological modelling in climate change impact studies in a Canadian, snow-dominated river basin, J. Hydrol., 409, 626–636, doi:10.1016/j.jhydrol.2011.08.057, 2011.
Prudhomme, C., Jakob, D., and Svensson, C.: Uncertainty and climate change impact on the flood regime of small UK catchments, J. Hydrol., 277, 1–23, 2003.
Quintana Seguí, P., Ribes, A., Martin, E., Habets, F., and Boé, J.: Comparison of three downscaling methods in simulating the impact of climate change on the hydrology of Mediterranean basins, J. Hydrol., 383, 111–124, doi:10.1016/j.jhydrol.2009.09.050, 2010.
Schmidli, J., Frei, C., and Vidale, P.-L.: Downscaling from GCM precipitation: a benchmark for dynamical and statistical downscaling methods, Int. J. Climatol., 26, 679–689, doi:10.1002/joc.1287, 2006.
Scinocca, J. F., McFarlane, N. A., Lazare, M., Li, J., and Plummer, D.: Technical Note: The CCCma third generation AGCM and its extension into the middle atmosphere, Atmos. Chem. Phys., 8, 7055–7074, doi:10.5194/acp-8-7055-2008, 2008.

HESSD
10, 14189–14227, 2013

Seiller, G., Anctil, F., and Perrin, C.: Multimodel evaluation of twenty lumped hydrological models under contrasted climate conditions, Hydrol. Earth Syst. Sci., 16, 1171–1189, doi:10.5194/hess-16-1171-2012, 2012.

Singh, V. P. and Xu, C.-Y.: Evaluation and generalization of 13 mass transfer equations for determining free water evaporation, Hydrol. Process., 11, 311–323, 1997.

Sugawara, M.: Automatic calibration of the tank model, Hydrol. Sci. Bull., 24, 375–388, 1979.

Teng, J., Vaze, J., Chiew, F. H. S., Wang, B., and Perraud, J.-M.: Estimating the relative uncertainties sourced from GCMs and hydrological models in modeling climate change impact on runoff, J. Hydrometeorol., 13, 122–139, doi:10.1175/JHM-D-11-058.1, 2012.

Thiery, D.: Utilisation d'un modèle global pour identifier sur un niveau piézométrique des influences multiples dues à diverses activités humaines, IAHS Publ. No. 136, Exeter, UK, 71–77, 1982.

Thornthwaite, C. W. and Mather, J. R.: The Water Balance. Publications in Climatology, Vol. VIII, No. 1., Drexel Institute of Climatology, Centerton, NJ, 104 pp., 1955.

Valéry, A.: Modélisation précipitations – débit sous influence nivale. Élaboration d'un module neige et évaluation sur 380 bassins versants, Agro Paris Tech., Paris, France, 417 pp., 2010.

Velázquez, J. A., Anctil, F., and Perrin, C.: Performance and reliability of multimodel hydrological ensemble simulations based on seventeen lumped models and a thousand catchments, Hydrol. Earth Syst. Sci., 14, 2303–2317, doi:10.5194/hess-14-2303-2010, 2010.

Velázquez, J. A., Schmid, J., Ricard, S., Muerth, M. J., Gauvin St-Denis, B., Minville, M., Chaumont, D., Caya, D., Ludwig, R., and Turcotte, R.: An ensemble approach to assess hydrological models' contribution to uncertainties in the analysis of climate change impact on water resources, Hydrol. Earth Syst. Sci., 17, 565–578, doi:10.5194/hess-17-565-2013, 2013.

Vicuna, S., Maurer, E. P., Joyce, B., Dracup, J. A., and Purkey, D.: The sensitivity of California water resources to climate change scenarios, J. Am. Water Resour. Assoc., 43, 482–498, doi:10.1111/j.1752-1688.2007.00038.x, 2007.

Wagener, T., Boyle, D. P., Lees, M. J., Wheater, H. S., Gupta, H. V., and Sorooshian, S.: A framework for development and application of hydrological models, Hydrol. Earth Syst. Sci., 5, 13–26, doi:10.5194/hess-5-13-2001, 2001.

Wang, Y. C., Yu, P. S., and Yang, T. C.: Comparison of genetic algorithms and shuffled complex evolution approach for calibrating distributed rainfall-runoff model, Hydrol. Process., 24, 1015–1026, doi:10.1002/hyp.7543, 2009.

Warmerdam, P. M. M., Kole, J., and Chormanski, J.: Modelling rainfall–runoff processes in the Hupselse Beek research basin, in: Ecohydrological Processes in Small Basins, Proceedings of the Strasbourg Conference, 24–26 September 1996, IHP-V, Technical Documents in Hydrology no. 14, UNESCO, Paris, 155–160, 1997.

Wilks, D. S.: Statistical Methods in the Atmospheric Sciences: An introduction, Academic press, San Diego, CA., 467 pp., 1995.

Xu, C.-Y. and Singh, V. P.: Dependence of evaporation on meteorological variables at different time-scales and intercomparison of estimation methods, Hydrol. Process., 12, 429–442, 1998.

Xu, C.-Y. and Singh, V. P.: Evaluation and generalization of radiation-based methods for calculating evaporation, Hydrol. Process., 14, 339–349, doi:10.1002/(SICI)1099-1085(20000215)14:2<339::AID-HYP928>3.0.CO;2-O, 2000.

Xu, C.-Y. and Singh, V. P.: Evaluation and generalization of temperature-based methods for calculating evaporation, Hydrol. Process., 15, 305–319, doi:10.1002/hyp.119, 2001.

Xu, C.-Y. and Singh, V. P.: Cross comparison of empirical equations for calculating potential evapotranspiration with data from Switzerland, Water Resour. Manag., 16, 197–219, 2002.

Zhao, R. J., Zuang, Y. L., Fang, L. R., and Zhang, Q. S.: The Xinanjiang model, IAHS Publ. No. 129, Oxford, UK, 351–356, 1980.

Table 1. List of the twenty lumped conceptual models and their source of inspiration.

Name	Acronym	Free parameters	Storages	Inspired by
M01	BUCK	6	3	BUCKET (Thornthwaite et Mather, 1955)
M02	CEQU	9	2	CEQUEAU (Girard et al., 1972)
M03	CRE0	6	3	CREC (Cormary et Guilbot, 1973)
M04	GARD	6	3	GARDENIA (Thiery, 1982)
M05	GR4J	4	3	GR4J (Perrin et al., 2003)
M06	HBV0	9	3	HBV (Bergström et al., 1973)
M07	HYMO	6	5	HYMOD (Wagener et al., 2001)
M08	IHAC	7	3	IHACRES (Jakeman et al., 1990)
M09	MART	7	4	MARTINE (Mazenc et al., 1984)
M10	MOHY	7	3	MOHYSE (Fortin et al., 2007)
M11	MORD	6	4	MORDOR (Garçon, 1999)
M12	NAM0	10	7	NAM (Nielsen et Hansen, 1973)
M13	PDM0	8	4	PDM (Moore et Clarke, 1981)
M14	SACR	9	5	SACRAMENTO (Burnash et al., 1973)
M15	SIMH	8	4	SIMHYD (Chiew et Siriwardena, 2005)
M16	SMAR	8	4	SMARY et SMARG (O'Connell et al., 1970)
M17	TAN0	7	4	TANK (Sugawara, 1979)
M18	TOPM	7	4	TOPMODEL (Beven et Kirkby, 1979)
M19	WAGE	8	3	WAGENINGEN (Warmerdam et al., 1997)
M20	XINA	8	5	XINANJIANG (Zhao et al., 1980)

HESSD
10, 14189–14227, 2013

Table 2. List of the seven snow module versions and free-parameters.

Name	Free parameters	Version details
N1	2	Initial CemaNeige version (Valéry, 2010) P1: C_{Tg}; P2: K_f
N2	4	Modified version (sinusoidal K_f, $T_f = -1\,^\circ C$, modified SnowFrac function, eT_G depending on air temp., progressive melt, free TG_{thresh}) P1: C_{Tg}; P2: min K_f; P3: max K_f; P4: TG_{thresh}
N3	5	Modified version (linear SnowFrac with free parameters added, free thermal coeff C_t) P1: CoeffG; P2: K_f; P3: C_t; P4: int; P5: T_{50}
N4	4	Modified version (modified SnowFrac function, free thermal coeff C_t, free G_{thresh}) P1: C_{Tg}; P2: K_f; P3: C_t; P4: G_{thresh}
N5	5	Modified version ($T_f = -1\,^\circ C$, sinusoidal K_f, modified SnowFrac function, free thermal coeff C_t, eT_G depending on air temp., progressive melt, free TG_{thresh}) P1: C_{Tg}; P2: min K_f; P3: max K_f; P4: C_t; P5: TG_{thresh}
N6	1	Modified version (modified SnowFrac function, eT_G not used) P1: K_f
N7	2	Modified version (50 layers, sinusoidal K_f, modified SnowFrac function) P1: C_{Tg}; P2: K_f

HESSD
10, 14189–14227, 2013
Climate change impacts on the hydrologic regime of a Canadian river
G. Seiller and F. Anctil

Table 3. Characteristics of the calibration performance (NSE_{sqrt}) pooled by hydrological models, PET formulations, and snow modules.

Hydrological model		PET formulation		Snow module	
Name	Median (5th, 95th)	Name	Median (5th, 95th)	Name	Median (5th, 95th)
M01	0.76 (0.67, 0.79)	E01	0.76 (0.56, 0.80)	N1	0.75 (0.53, 0.81)
M02	0.56 (0.48, 0.62)	E02	0.70 (0.50, 0.78)	N2	0.75 (0.53, 0.81)
M03	0.78 (0.70, 0.80)	E03	0.75 (0.55, 0.79)	N3	0.75 (0.55, 0.81)
M04	0.77 (0.68, 0.79)	E04	0.76 (0.58, 0.81)	N4	0.75 (0.55, 0.80)
M05	0.81 (0.72, 0.83)	E05	0.76 (0.55, 0.80)	N5	0.75 (0.52, 0.80)
M06	0.76 (0.69, 0.78)	E06	0.75 (0.56, 0.79)	N6	0.75 (0.56, 0.80)
M07	0.60 (0.49, 0.63)	E07	0.77 (0.60, 0.82)	N7	0.71 (0.52, 0.79)
M08	0.71 (0.64, 0.75)	E08	0.68 (0.47, 0.78)		
M09	0.76 (0.64, 0.80)	E09	0.76 (0.53, 0.81)		
M10	0.73 (0.58, 0.81)	E10	0.67 (0.49, 0.72)		
M11	0.74 (0.63, 0.80)	E11	0.74 (0.54, 0.80)		
M12	0.71 (0.36, 0.78)	E12	0.66 (0.45, 0.79)		
M13	0.57 (0.47, 0.65)	E13	0.77 (0.58, 0.81)		
M14	0.78 (0.68, 0.81)	E14	0.77 (0.61, 0.81)		
M15	0.75 (0.62, 0.79)	E15	0.75 (0.56, 0.79)		
M16	0.78 (0.68, 0.80)	E16	0.76 (0.58, 0.81)		
M17	0.76 (0.68, 0.80)	E17	0.75 (0.56, 0.80)		
M18	0.77 (0.67, 0.80)	E18	0.77 (0.59, 0.80)		
M19	0.76 (0.65, 0.81)	E19	0.75 (0.56, 0.81)		
M20	0.63 (0.56, 0.65)	E20	0.72 (0.54, 0.80)		
		E21	0.69 (0.49, 0.76)		
		E22	0.77 (0.57, 0.81)		
		E23	0.78 (0.59, 0.82)		
		E24	0.77 (0.59, 0.82)		

HESSD
10, 14189–14227, 2013

Table 4. Characteristics of the median OMF relative change for different processes and periods.

	Lowest value	Highest value	Standard deviation
OMF			
Hydrological model	+6.3 % (M02)	+16.8 % (M08)	2.4 %
PET formulation	+4.1 % (E13)	+17.1 % (E21)	3.3 %
Snow module	+9.1 % (N2)	+9.9 % (N3)	0.3 %
Climatic member	+2.7 % (C4)	+19.1 % (C3)	6.9 %
Apr to Oct OMF			
Hydrological model	−14.2 % (M06)	−4.1 % (M08)	2.4 %
PET formulation	−15.8 % (E14)	−1.7 % (E21)	3.1 %
Snow module	−11.3 % (N1)	−10.1 % (N6)	0.5 %
Climatic member	−19.5 % (C2)	−2.4 % (C3)	7.6 %
Nov to May OMF			
Hydrological model	+17.1 % (M17)	+27.5 % (M08)	2.1 %
PET formulation	+14.1 % (E14)	+32.2 % (E21)	4.0 %
Snow module	+20.5 % (N1)	+21.1 % (N6)	0.3 %
Climatic member	+15.7 % (C4)	+26.3 % (C3)	4.7 %

HESSD
10, 14189–14227, 2013

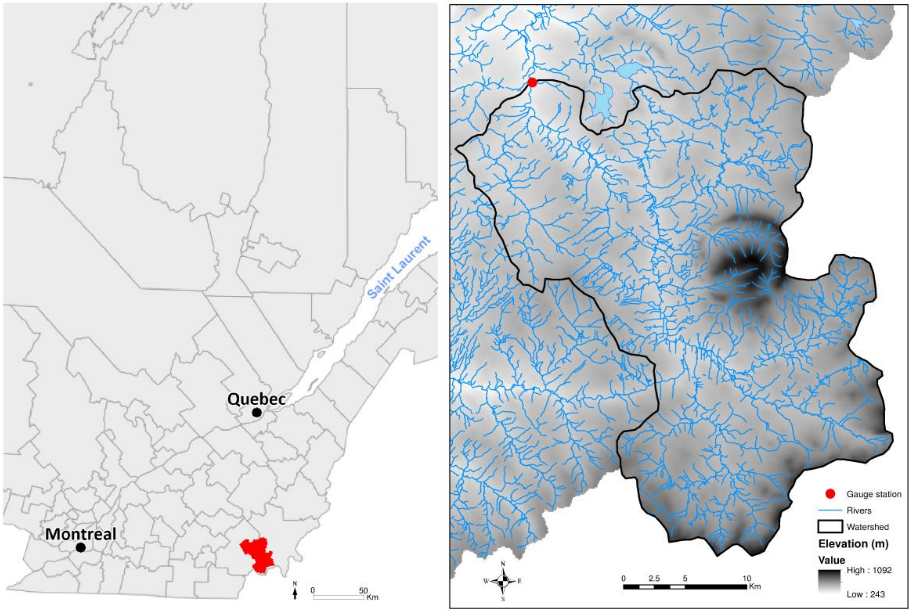

Fig. 1. Localisation of the *au Saumon* catchment (738 km^2; Canada).

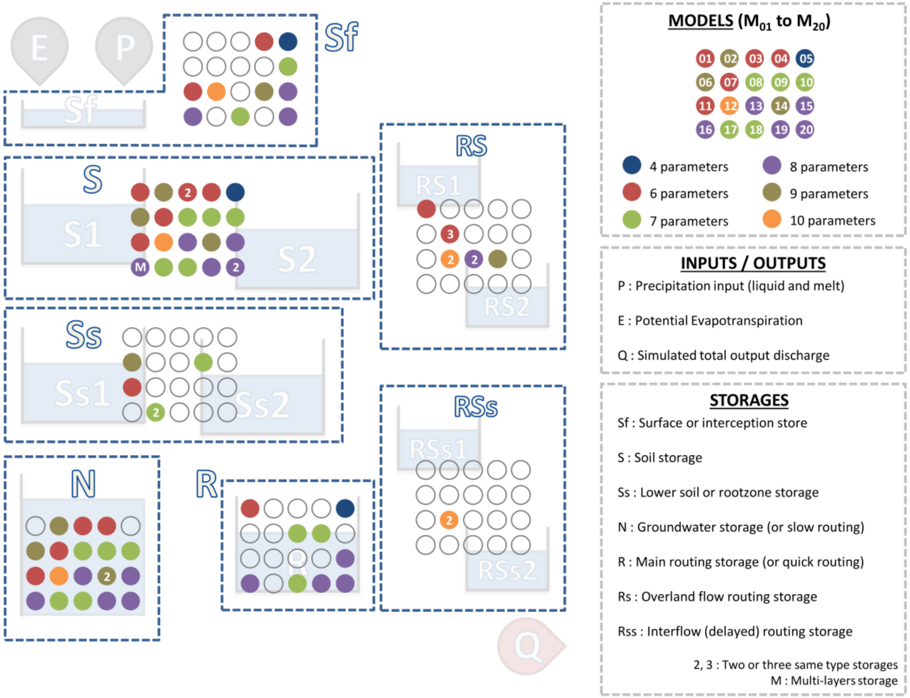

Fig. 2. Illustration of the structural diversity of the twenty lumped conceptual models.

HESSD
10, 14189–14227, 2013

Climate change impacts on the hydrologic regime of a Canadian river

G. Seiller and F. Anctil

Combinational	Data
1.Penman	RH, T, U, Rs
2.Penman-Monteith	RH, T, U, Rs
3.FAO56 P-M (ASCE)	RH, T, U, Rs
4.Priestley-Taylor	T, Rs
5.Kimberly-Penman	RH, T, U, Rs
6.Thom-Oliver	RH, T, U, Rs

Temperature	Data
7.Thornthwaite	T
8.Blaney-Criddle	T, Rs
9.Hamon	T, Rs
10.Romanenko	RH, T
11.Linacre	RH, T
12.MOHYSE	T
13.Hydro-Qc (HSAMI)	T
14.Kharrufa	T

Radiation	Data
15.Wendling (WASim)	T, Rs
16.Turc	RH, T, Rs
17.Jensen-Haise	T
18.McGuinness-Bordne	T
19.Hargreaves	T
20.Doorenbos-Pruitt	RH, T, U, Rs
21.Abtew	RH, T, Rs
22.Makkink	T
23.Oudin	T
24.Baier-Robertson	T

RH : Relative humidity
T : Temperature
U : Wind speed
Rs : Incoming solar radiation

Fig. 3. List of the twenty-four PET formulations per category: combinational, temperature-based, and radiation-based.

HESSD
10, 14189–14227, 2013

Climate change impacts on the hydrologic regime of a Canadian river

G. Seiller and F. Anctil

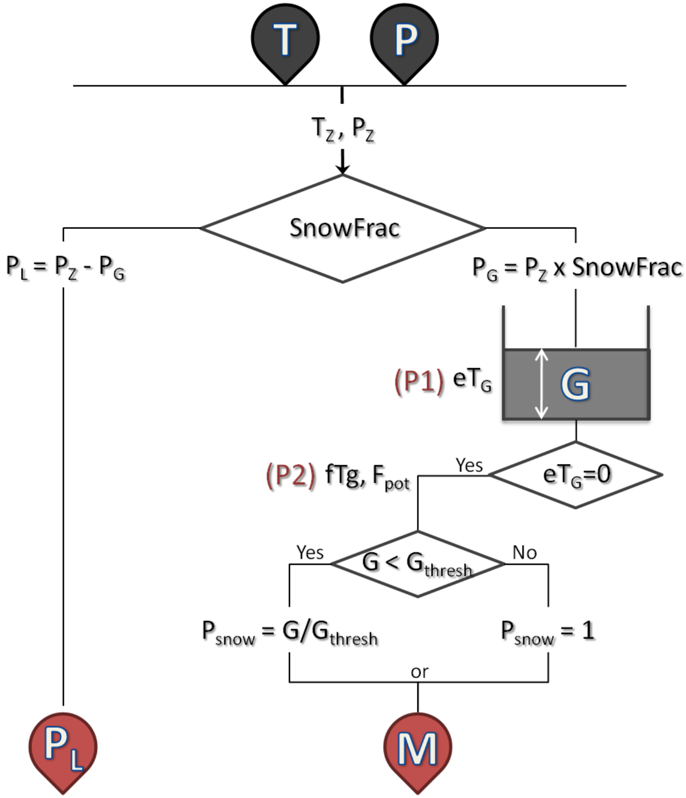

Fig. 4. Initial version of the CemaNeige snow module (N1). *T* is temperature, *P* is total precipitation, P_L is liquid precipitation, and *M* is snowmelt. *G* corresponds to the snowpack and P1 and P2 are the two free parameters (inspired from Valéry, 2010).

HESSD
10, 14189–14227, 2013

Climate change impacts on the hydrologic regime of a Canadian river

G. Seiller and F. Anctil

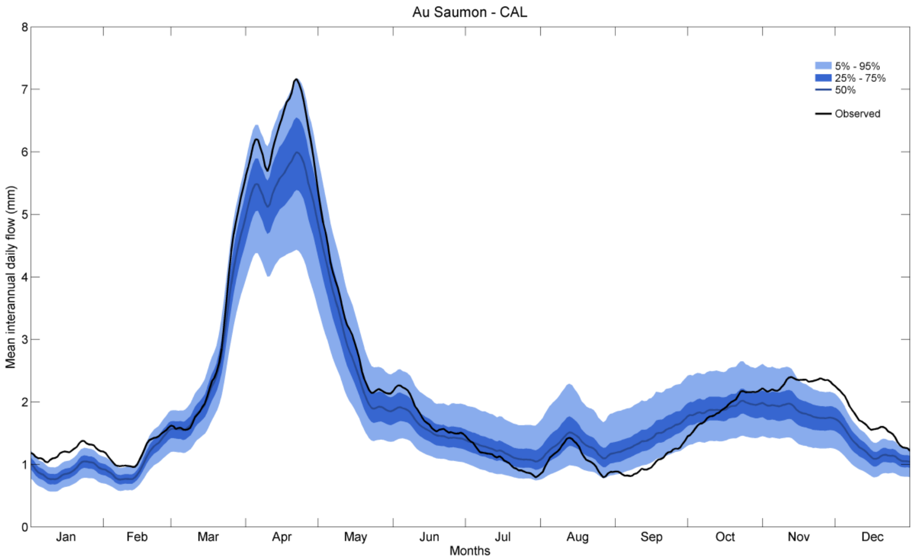

Fig. 5. Cumulative uncertainties for the observed period simulation. The black line is the observed flow, the blue line depicts the median flow simulation, and the dark and pale blue envelopes, the distribution of the streamflow ensemble (5 % to 95 % and 25 % to 75 %, respectively).

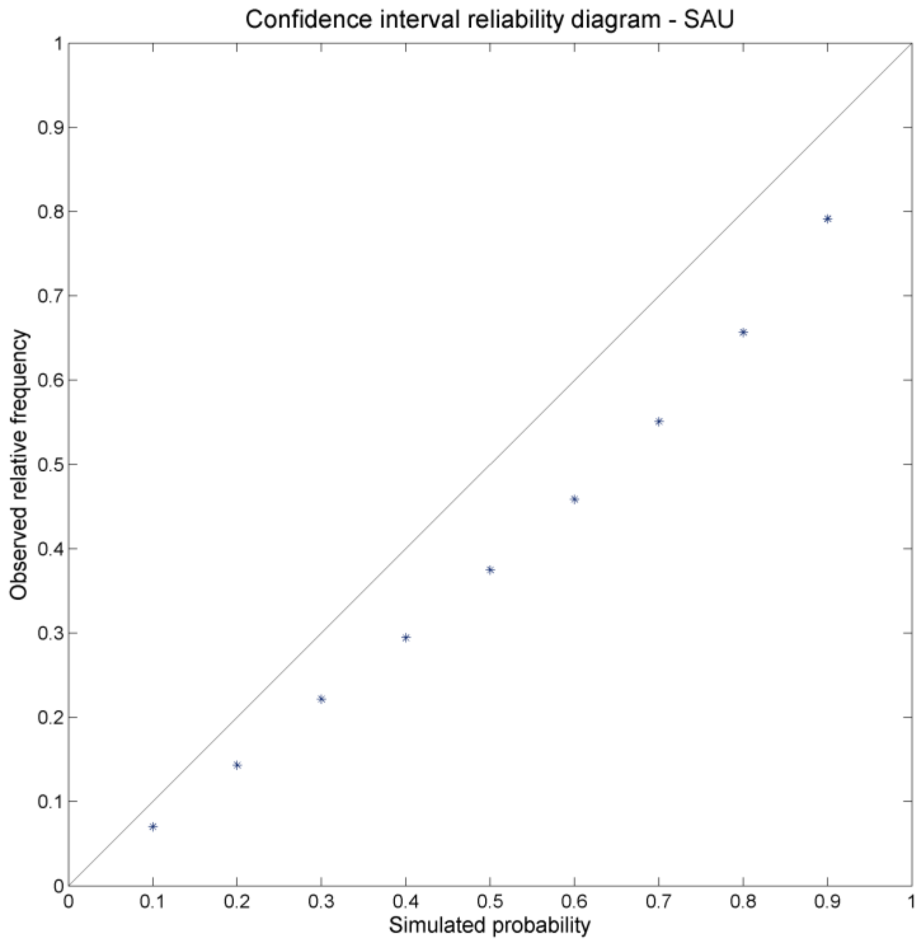

Fig. 6. Confidence interval reliability diagram opposing simulated probability (x-axis) and observed relative frequency (y-axis).

HESSD
10, 14189–14227, 2013

G. Seiller and F. Anctil

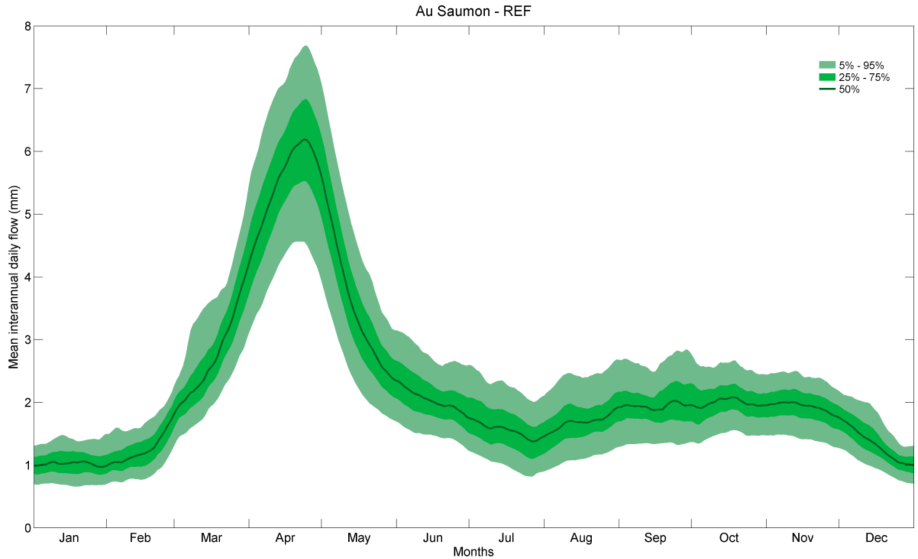

Fig. 7. Cumulative uncertainties of the reference (REF) simulations. The line depicts the median flow simulation and the dark and pale green envelopes, the distribution of the streamflow ensemble (5 % to 95 % and 25 % to 75 %, respectively).

HESSD
10, 14189–14227, 2013

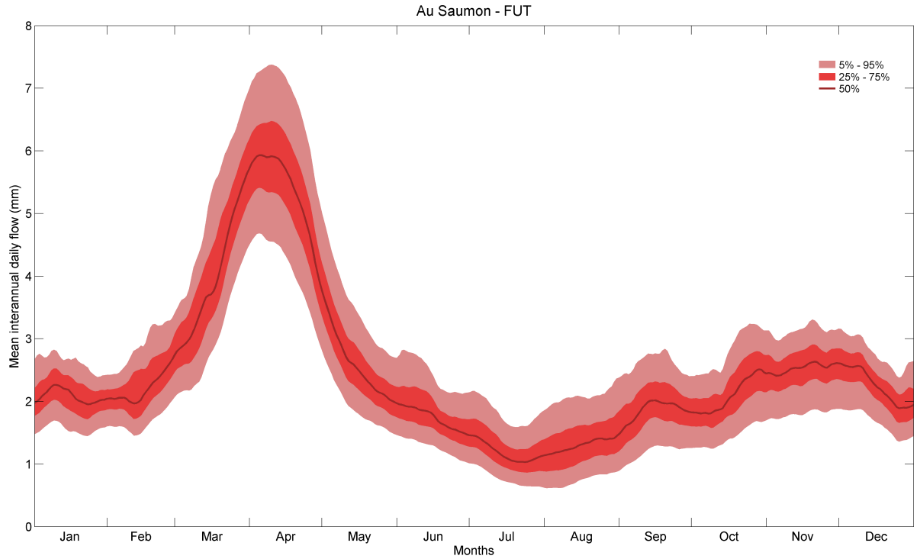

Fig. 8. Cumulative uncertainties of the future (FUT) projection. The line depicts the median flow projection and the dark and pale red envelopes, the distribution of the streamflow ensemble (5 % to 95 % and 25 % to 75 %, respectively).

HESSD
10, 14189–14227, 2013

Climate change impacts on the hydrologic regime of a Canadian river

G. Seiller and F. Anctil

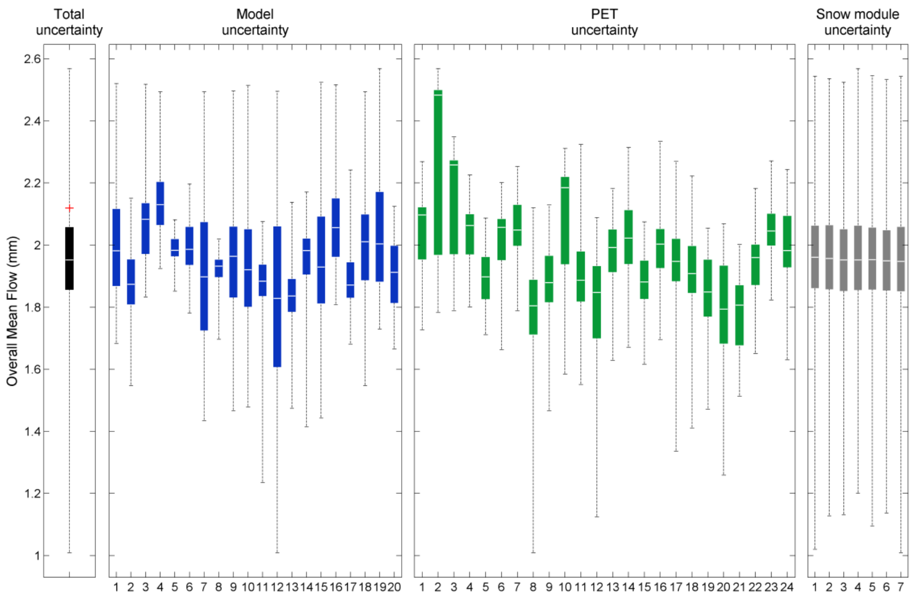

Fig. 9. Total and process-based overall mean flow (OMF, mm) uncertainty, for simulation on the observed period. The observed OMF is illustrated by a red cross in the total uncertainty box.

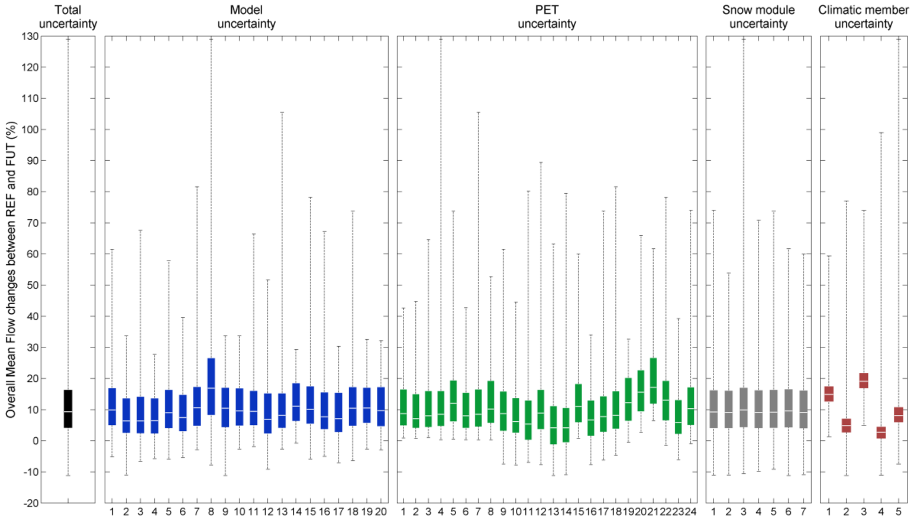

Fig. 10. Total, process-based, and natural climate overall mean flow evolution (from REF to FUT, %) uncertainty.

HESSD
10, 14189–14227, 2013

G. Seiller and F. Anctil